metals

MDPI

Article

Rapid Annealing Optimizing Magnetic Softness and Thermal Stability of Mn-Substituted Fe-Based Nanocrystalline Alloys

Bojun Zhang [1], Fuyao Yang [2], Aina He [1,3,*], Huiyun Xiao [1,3], Yaqiang Dong [1,3], Jiawei Li [1,3,*] and Yu Han [2]

[1] CAS Key Laboratory of Magnetic Materials and Devices, Zhejiang Province Key Laboratory of Magnetic Materials and Application Technology, Ningbo Institute of Materials Technology and Engineering, Chinese Academy of Sciences, Ningbo 315201, Zhejiang, China; zhangbojun@nimte.ac.cn (B.Z.); xiaohuiyun@nimte.ac.cn (H.X.); dongyq@nimte.ac.cn (Y.D.)
[2] State Key Laboratory of Advanced Power Transmission Technology, Global Energy Interconnection Research Institute Co., Ltd., Beijing 102211, China; yfy55555@sina.com (F.Y.); epri313@sina.com (Y.H.)
[3] Department of Materials Engineering, University of Chinese Academy of Sciences, Beijing 100049, China
* Correspondence: hean@nimte.ac.cn (A.H.); lijw@nimte.ac.cn (J.L.); Tel.: +86-574-8761-7212 (J.L.)

Abstract: Good high-frequency magnetic softness and thermal stability are very important for the wide application of Fe-based nanocrystalline alloys. The present work reports the influence of Mn-doping and rapid annealing on the magnetic softness, nano-structure, and magnetic-microstructure of $Fe_{76-x}Si_{13}B_8Nb_2Cu_1Mn_x$ (x = 0, 1, 2, 3, and 4) alloys. It was found that the $Fe_{74}Si_{13}B_8Nb_2Cu_1Mn_2$ alloy exhibits a superior magnetic softness with the high-saturation magnetic induction of 1.32 T and a large permeability at 100 kHz of over 15,000 at a large annealing-temperature region of 120 °C. The microstructure and magnetic domains characterization indicate that the good magnetic softness and thermal stabilization can be ascribed to the superb nano-structural stability caused by the Mn doping and rapid annealing at elongated temperatures, which can maintain a fine and high number density α-Fe(Si) nano-grains and facilitate the formation of regular and wide domains.

Keywords: nanocrystalline alloy; high frequency; magnetic softness; magnetic domain; rapid annealing

Citation: Zhang, B.; Yang, F.; He, A.; Xiao, H.; Dong, Y.; Li, J. Rapid Annealing Optimizing Magnetic Softness and Thermal Stability of Mn-Substituted Fe-Based Nanocrystalline Alloys. *Metals* **2021**, *11*, 20. https://doi.org/10.3390/met11010020

Received: 19 November 2020
Accepted: 17 December 2020
Published: 24 December 2020

1. Introduction

Due to high saturation magnetic induction (B_s), large high-frequency permeability (μ), and small high-frequency loss (P), Fe-based nanocrystalline alloys are gradually replacing permalloy and soft-ferrite and are widely applied in filter inductions, high-frequency transformers/inverters, and leakage short-circuit devices, etc. [1,2]. Finemet ® alloys (representative composition $Fe_{73.5}Si_{13.5}B_9Nb_3Cu_1$) with an excellent comprehensive magnetic softness were first discovered by Yoshizawa et al. in 1988 [3], and are still the most widely used nanocrystalline alloys so far. However, their low B_s of around 1.24 T is not conducive to the miniaturization and high power of electromagnetic devices. Many efforts have been devoted to improve the B_s of Fe-based nanocrystalline alloys—e.g., increasing the Fe content [4–6], adding Co element to increase the magnetic exchange interaction [7–9], decreasing the amount non-magnetic and large-sized elements [10,11], and removing Cu element [12,13]. However, these alloys with high B_s suffer from a low amorphous-forming ability and poor high-frequency magnetic softness, which is unable to meet the requirement for mass production and high-frequency applications. Therefore, it is of paramount importance to simultaneously improve their B_s and high-frequency magnetic performance.

Rapid annealing (RA) has been found to be an effective strategy for refining nanograins, promoting crystallinity and reducing coercivity (H_c) and P in the high-B_s nanocrystalline alloys such as Fe-B-(Cu, Ni) [14,15], Fe-Nb-B-(Cu) [16], and Fe-Si-B-Nb-(Cu)

[17,18], as well as Fe-Si-B-P-C-Cu [19]. Despite the longstanding interest in RA for improving static magnetic softness and lowering core loss at a low frequency, there are only few studies on the correction between high-frequency magnetic softness (e.g., μ at 100 kHz) and RA, which needs further investigation and is of great importance in understanding their microstructure–properties relationship.

In our previous work, a representative $Fe_{76}Si_{13}B_8Nb_2Cu_1$ nanocrystalline alloy with a good magnetic softness and manufacturability was developed [20,21]. Compared with non-magnetic metals, Mn has less negative influence on B_s and can increase the crystalline volume fraction and thermal stability of the nanocrystalline alloys [22–24], while the magnetic softness is not improved by normal-annealing (NA). Herein, with aim of improving the soft magnetic performance and thermal stability, the effects of Mn doping and RA on the thermal properties, high-frequency magnetic softness, microstructure, and magnetic domains of $Fe_{76}Si_{13}B_8Nb_2Cu_1$ nanocrystalline alloy have been investigated in detail. The RA alloy exhibits a high B_s, good high-frequency permeability, and wide annealing-temperature region, making it very suitable for high-power and high-frequency devices.

2. Experimental Procedures

Master alloys with nominal atomic compositions of $Fe_{76-x}Si_{13}B_8Nb_2Cu_1Mn_x$ (x = 0, 1, 2, 3, and 4) were prepared by induction melting with the mixtures of pure Fe (99.99 mass%), Si (99.99 mass%), B (99.9 mass%), Cu (99.99 mass%), and Mn (99.9 mass%). The as-quenched ribbons with a width of about 1 mm and a thickness of about 26 μm were prepared by a single-roller melt-spinning method at a spinning rate of 45 m/s. Then, the as-quenched ribbons were heat treated at 480 ~ 640 °C for 10 min in a rapid annealing (RA) furnace, in which the heating rate was up to 300 °C/min. For comparison, the normal-annealing (NA) was conducted in a tube furnace with a vacuum of about 5×10^{-3} Pa.

Thermal parameters such as the onset crystallization temperature (T_{x1}, T_{x2}) and the temperature interval ($\Delta T = T_{x2} - T_{x1}$) were examined by differential scanning calorimetry (DSC, NETZSCH 404C, Selb, Germany) at a heating rate of 40 °C/min. Melting and solidification behaviors were observed via the DSC at a heating rate of 40 °C/min and a cooling rate of 4 °C/min, respectively. Magnetic softness, including the H_c, μ, and B_s, was measured via a DC *B-H* loop tracer (EXPH-100, Riken Deshi Co., Ltd., Saitama, Japan) under the maximum applied field of 800 A/m, an impedance analyzer (Agilent 4294 A, PaloAlto, CA, USA) with an AC magnetic field magnitude (H_m) of 1~50 A/m and a frequency of 1 kHz ~ 100 MHz, as well as a vibrating sample magnetometer (VSM, Lake Shore 7410, Columbus, OH, USA) under the maximum applied field of 800 kA/m, respectively. The microstructure and precipitation phases of the as-quenched and annealed samples were first identified by X-ray diffraction (XRD, Bruker D8 Advance, Karlsruhe, Germany) with Cu-Kα radiation. The nano-structure of the annealed samples was further characterized by transmission electron microscopy (TEM, Talos F200x, Hillsboro, OR, USA), and the TEM samples were prepared by ion-milling (Gatan691, Gatan, Pleasanton, CA, USA). The magnetic domain structure was obtained by magneto-optical Kerr microscopy (4-873K/950MT, Germany).

3. Results and Discussion

The influences of Mn on the melting and solidification processes, amorphous forming ability, and crystallization characterization of $Fe_{76-x}Si_{13}B_8Nb_2Cu_1Mn_x$ (x = 0, 1, 2, 3, and 4) alloys were first investigated. The ribbons with x = 0, 1, 2, 3, and 4 are conveniently labeled as Mn0, Mn1, Mn2, Mn3, and Mn4, respectively. As shown in Figure 1a,b, the onset temperature of the melting endothermic peak (T_m) and the solidification exothermic peak (T_{ls}) slightly shifts to a lower temperature with the increasing Mn content, suggesting that the substitution of Mn (≤4 at.%) for Fe has no obvious influence on the melting and solidification behaviors of FeSiBNbCu master alloys. According to the XRD pattern in Figure 1c, all as-quenched ribbons exhibit a fully amorphous structure characterized by only a halo peak at 2θ of about 45°. Figure 1d displays the DSC curves of the as-quenched

ribbons. The crystallization of the ribbons happens in 2~3 stages. The T_{x1} and T_{x2} corresponding to the onset temperature for the precipitation of the α-Fe(Si) phase and the precipitation of iron borides [25] slightly shifts to a high and low temperature side, respectively. Since the mixing enthalpy between Cu and Fe is positive (13 kJ/mol) while that between Cu and Mn is negative (−6 kJ/mol) [26], the driving force for Cu clustering is thus reduced when replacing Mn for Fe. This would be responsible for the slight improvement in T_{x1}. It is noteworthy that the Mn-doping alloys exhibit a wide ΔT (= T_{x2} − T_{x1}) above 145 °C, which is comparable to the commercial Finemet® alloys [27], suggesting the facile formation of α-Fe(Si) nano-grains and good thermal stability of the residual amorphous matrix.

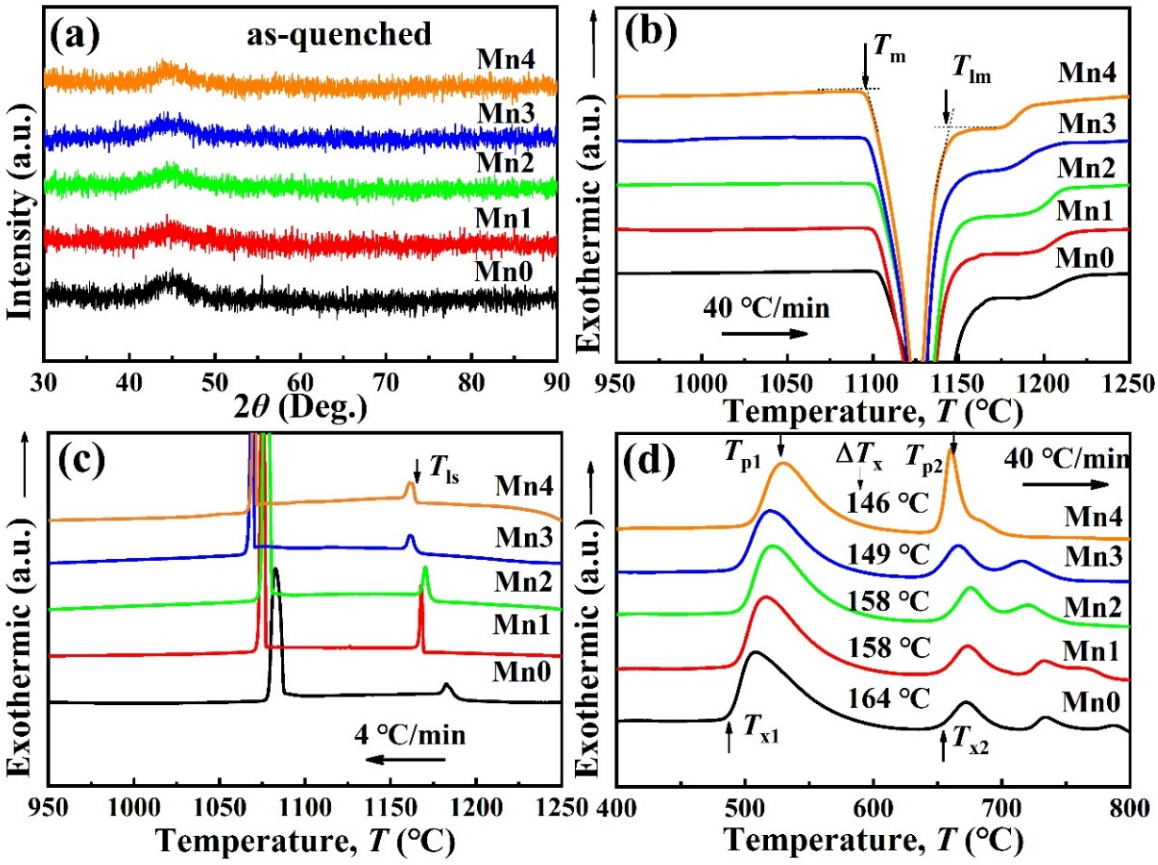

Figure 1. Thermal and structural characteristics of Mn0, Mn1, Mn2, Mn3, and Mn4. (**a**) XRD patterns of the as-quenched ribbons, showing a fully amorphous structure; DSC curves of the (**b**) heating and (**c**) cooling of master alloys, showing the melting and solidification processes; (**d**) DSC curves of the as-quenched ribbons, showing a large ΔT of 146 ~ 164 °C.

The magnetic softness of Mn0, Mn1, Mn2, Mn3 and, Mn4 annealed in an FA process was investigated by measuring the H_c, μ, and B_s. As shown in Figure 2a, Mn1 and Mn2 exhibit a low H_c of 1.1~1.8 A/m at a large annealing temperature (T_a) region of 480~600 °C, which is better than that of the other alloys. Moreover, as the T_a rises up to 600 °C, the H_c of Mn2 is still below 10 A/m, while that of the other four alloys deteriorates to over 100 A/m. For Mn2, μ at 100 kHz keeps a high value of above 15,000 at a wide T_a range of 480~600 °C and slightly decreases to 9200 at 640 °C. Whereas, the μ at 100 kHz of the other alloys decreases starting from 600 °C, and sharply decreases to below 1000 at 640 °C. These results indicate that Mn2 exhibits a superior thermal stability for obtaining an excellent magnetic softness. The dependence of μ at 1A/m on the frequency and the dependence of μ at 100 kHz on the AC magnetic field magnitude (H_m) of Mn0, Mn1, Mn2, Mn3, and Mn4 annealed at 600 °C were tested to analyze the high-frequency characterization, as presented in Figure 2c,d, respectively. As the frequency increases, μ stays constant at low and

medium frequencies, and subsequently reduces at higher frequencies, as shown in Figure 2c. As the frequency increases, the magnetic domain walls and magnetization would become more difficult to move and rotate, which results in a decrease in their contribution, leading to a decrease in μ [28]. The μ at 100 kHz of Mn2 is independent of H_m (Figure 2d), suggesting a good magnetic saturation resistance which is different from that of the other alloys. Therefore, the substitution of Mn with a proper content for Fe could effectively reduce H_c, enhance high-frequency μ, enlarge the optimal T_a range, and improve the magnetic-saturation resistance.

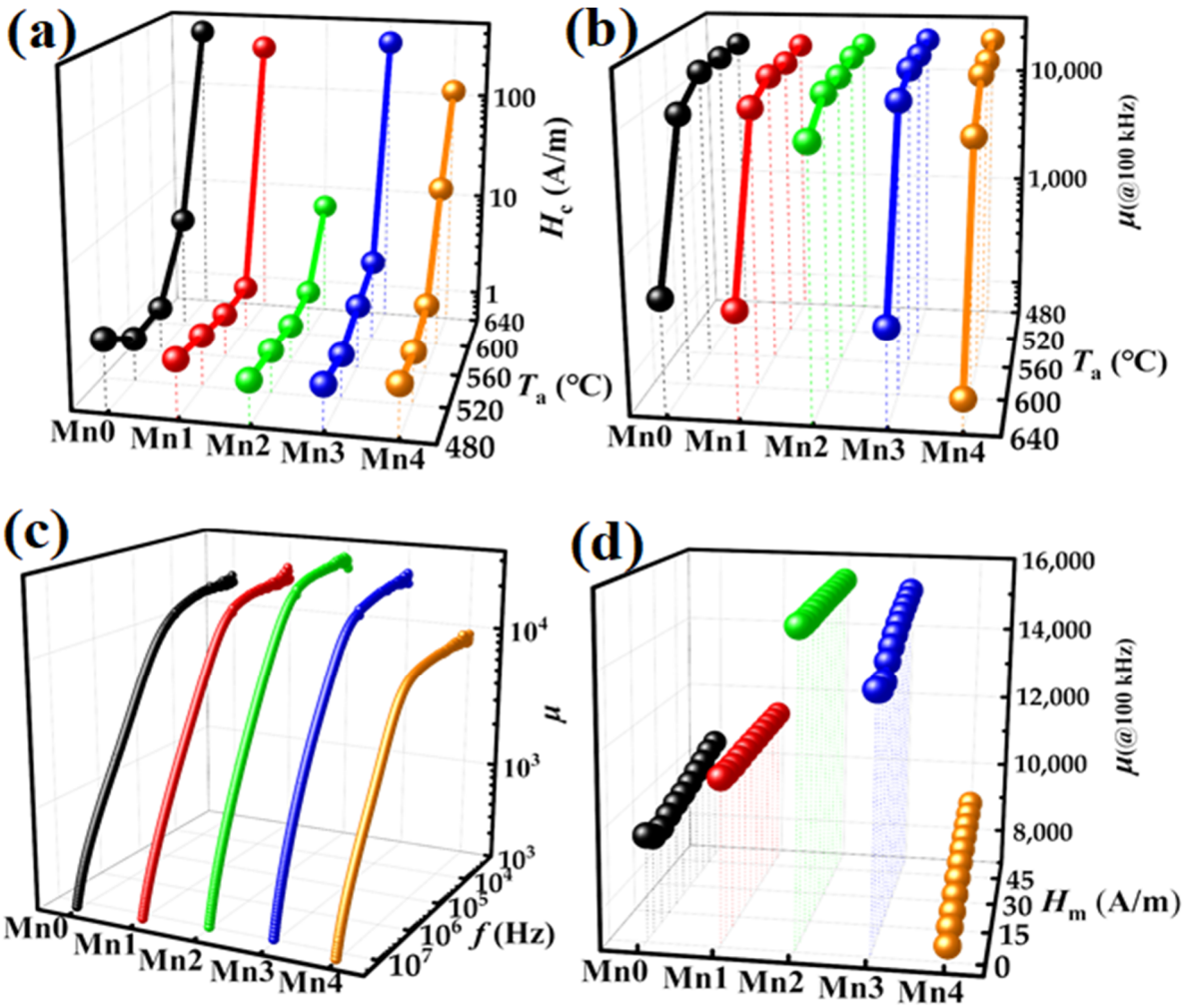

Figure 2. Magnetic softness of Mn0, Mn1, Mn2, Mn3, and Mn4 by RA. T_a dependence of (**a**) H_c and (**b**) μ at 100 kHz and 1 A/m, (**c**) frequency dependence of μ at 1 A/m for the ribbons treated at 600 °C, (**d**) AC magnetic field magnitude (H_m) dependence of μ at 100 kHz for the ribbons treated at 600 °C.

The hysteresis loops of Mn0, Mn1, Mn2, Mn3, and Mn4 annealed at an optimum T_a were then performed via the VSM. As shown in Figure 3, all the alloys depict typical loops of nanocrystalline soft magnetic materials. The B_s decreases with the increase in Mn content, but is still greater than the typical B_s (1.24 T) of the Finemet ® alloys. For example, the B_s of Mn2 is 1.33 T, which is 7% higher than that of the Finemet ® alloys. Therefore, the substitution of Mn for Fe does not significantly reduce B_s. The large B_s, good high-frequency magnetic softness, wide ΔT and T_a range, as well as high magnetic-saturation resistance are combined in Mn2, which is beneficial to minimize the size, boost the power density, and improve the efficiency of magnetic devices.

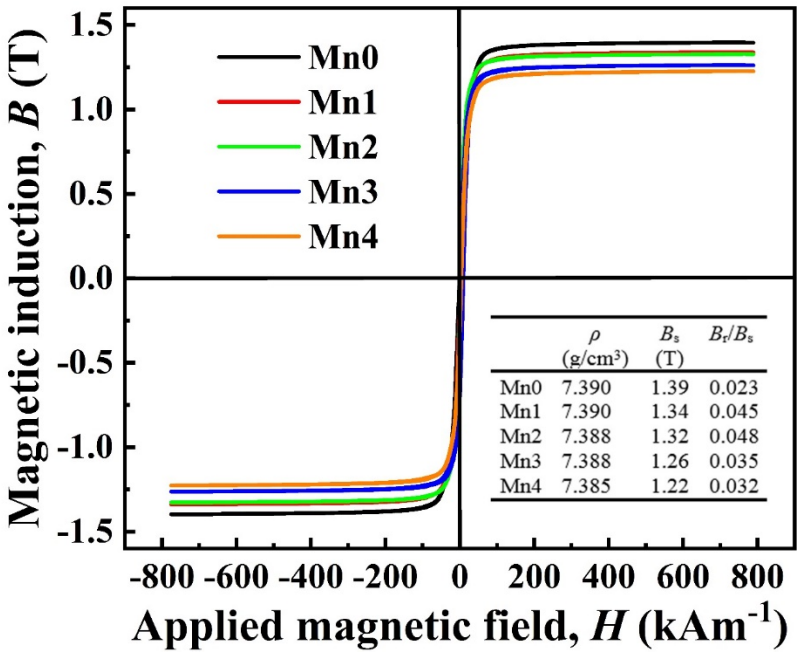

Figure 3. Hysteresis loops of Mn0, Mn1, Mn2, Mn3, and Mn4 annealed at optimal T_a. Inset shows the density (ρ), B_s, and B_r/B_s of the optimal Mn0, Mn1, Mn2, Mn3, and Mn4 alloys.

The H_c and high-frequency μ of Mn2 by RA and NA were compared to unveil the effect of the annealing heating rate on the magnetic softness and thermal stability, as shown in Table 1. Mn2 by RA exhibits a high μ at 100 kHz over 15,000 and a low H_c below 1.5 A/m at a wide T_a range of 480~600 °C. In contrast, the NA sample displays a higher H_c and a much lower μ at 100 kHz at all annealing conditions. In particular, the μ at 100 kHz of the RA sample exhibits an increase of 240% at 480 °C (close to T_{x1}) as compared with that of the NA sample. Therefore, RA can remarkably enhance high-frequency μ at 100 kHz and reduce H_c at a large annealing temperature window, manifesting the effectiveness of RA in improving the magnetic softness and thermal stability.

Table 1. μ at 100 kHz and H_c of Mn2 by RA and NA at different T_a.

Annealing	Annealing Temperature (T_a)							
	480 °C		520 °C		600 °C		640 °C	
	H_c (A/m)	μ @100 kHz	H_c (A/m)	μ @100 kHz	H_c (A/m)	μ @100 kHz	H_c (A/m)	μ @100 kHz
RA	1.3	15,900	1.3	16,000	1.4	15,700	6.0	9200
NA	3.5	4700	2.0	10,200	2.3	10,100	8.4	6400

To reveal the enhancement mechanism in high-frequency magnetic softness and thermal stability, the microstructures and their evolution processes of Mn2 by RA and NA at different T_a were subsequently investigated, as shown in Figure 4. Annealing at 480 °C (close to T_{x1}) generates a small peak at around $2\theta = 45°$ for NA, whereas it results in obvious crystallization for RA, identified by the sharp peaks at about $2\theta = 45°$, 65°, and 83°, respectively, corresponding to the α-Fe(Si) phase. After annealing at 600 °C (between T_{x1} and T_{x2}), both NA and RA cause an obvious crystallization verified by the sharp crystal peaks. According to the Scherrer equation [29], we calculated the average size of the α-Fe(Si) grains of the RA sample, which exhibits a plateau size of around 13 nm for a wide T_a interval of 120 °C. This behavior indicates the excellent thermal stability of Mn2 by RA. When T_a increases to 640 °C (close to T_{x2}), the Fe_3B phase can be detected for both the NA and RA samples, which is responsible for the deterioration of magnetic softness.

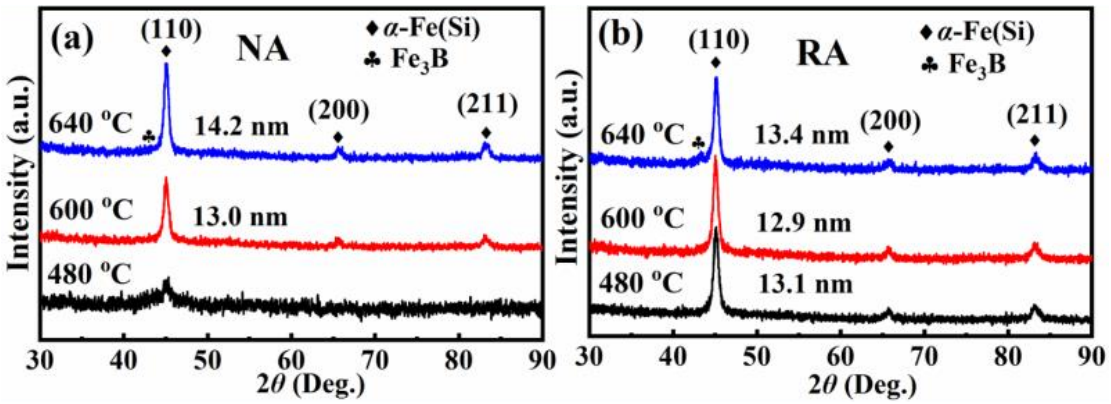

Figure 4. XRD patterns of Mn2 by (**a**) NA and (**b**) RA at different T_a.

To further analyze the changes in the microstructure, selected TEM bright-field images, SAED patterns, and grain size distributions of Mn2 after annealing at 480, 600, and 640 °C via NA and RA were obtained and are displayed in Figure 5. After annealing close to T_{x1}, NA causes a low number density of grains with the size of 11~17 nm embedded unevenly in a clearly visible amorphous region (Figure 5a,a_2). However, RA generates a high number density of grains with the size of around 12.5 nm distributed uniformly in a nearly invisible amorphous region (Figure 5b,b_2), demonstrating the effectiveness of RA in obtaining a superb nano-structure. These grains are identified as the α-Fe(Si) phase (Figure 5a_1,b_1), which is consistent with the XRD results. The uncompleted precipitation of α-Fe(Si) grains from the amorphous matrix of NA sample cannot effectively reduce the magneto-crystalline anisotropy by exchange interaction [2,30], which accounts for the inferior magnetic softness. After annealing at 600 °C (between T_{x1} and T_{x2}), both the NA and RA samples precipitate a large number of ultrafine α-Fe(Si) nano-grains from the amorphous matrix (Figure 5c,d). The RA samples annealed at 480 and 600 °C have similar grain size of around 12.6 nm, which is smaller than that of the NA sample annealed at 600 °C. The stable nanocrystalline structure caused by RA leads to the superb magnetic softness of Mn2 in a wide annealing temperature region of 120 °C, since the permeability is inversely proportional to six times the nano-grains size [2]. After annealing at 640 °C (near T_{x2}), Fe_3B phase with a large magnetic anisotropy precipitates from the amorphous matrix (Figure 5e_1,f_1). The Fe_3B nano-grains can pin magnetic domain walls, which account for the worsening of the magnetic softness [25].

Magnetic domain structures were also investigated to interpret the excellent magnetic softness of Mn2 by RA, as depicted in Figure 6. At 480 °C, irregular and small magnetic domains with many branches appear in the NA sample (Figure 6a), while the FA sample has relatively regular and wide domains (Figure 6c), which can essentially prove the low pinning effect and small magnetic anisotropy of the FA sample. At 600 °C, the NA sample has bent-edged and narrow domains, whereas the FA sample exhibits smooth-edged and wide domains, demonstrating the facile movement of the domain walls. FA generates high density, homogeneous, and ultrafine α-Fe(Si) nano-grains at 480–600 °C (Figure 5b,d), leading to an effective reduction in magnetic anisotropy due to the strong exchange interaction, and finally enabling the formation of regular and wide domains in a large annealing temperature region. This is responsible for the superb magnetic softness and thermal stability of Mn2 by RA.

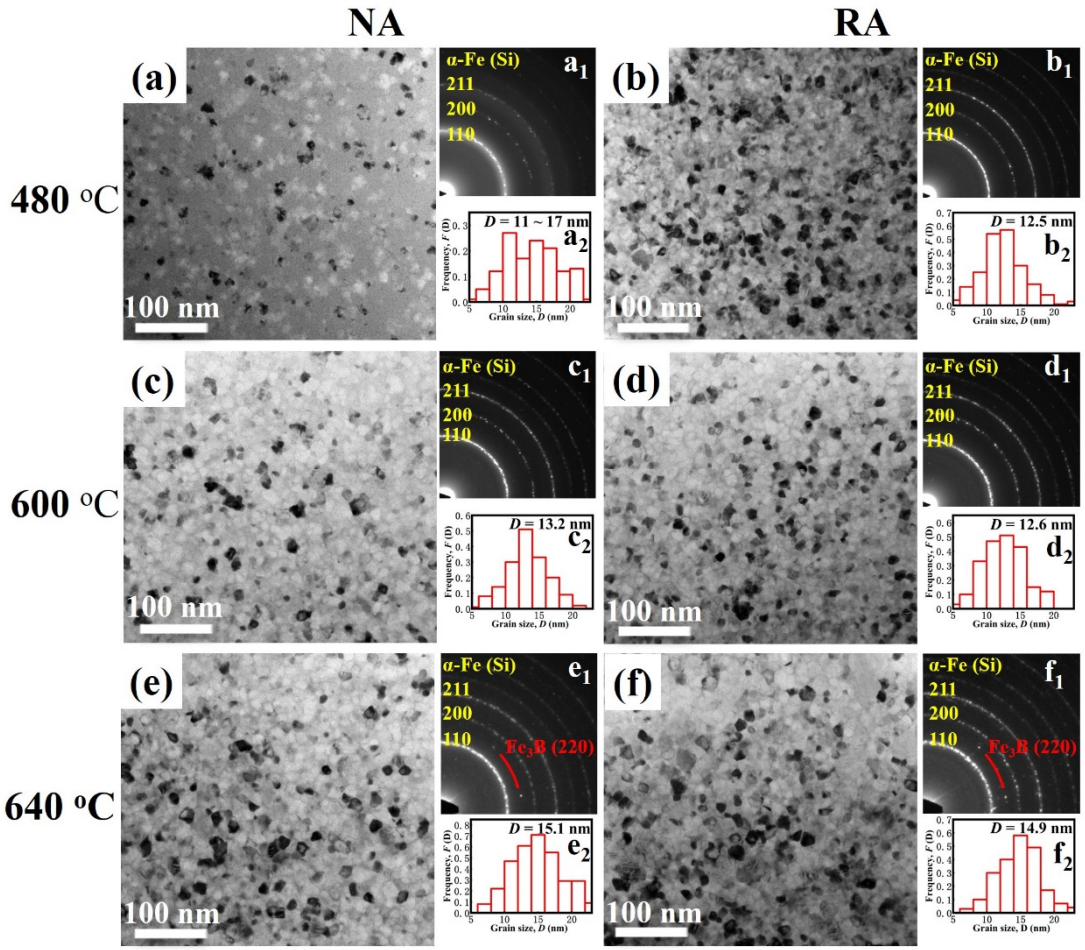

Figure 5. TEM bright-field images, SAED patterns, and grain size distribution of Mn2 annealed at 480, 600, and 640 °C via (**a**,**c**,**e**) NA and (**b**,**d**,**f**) RA, respectively.

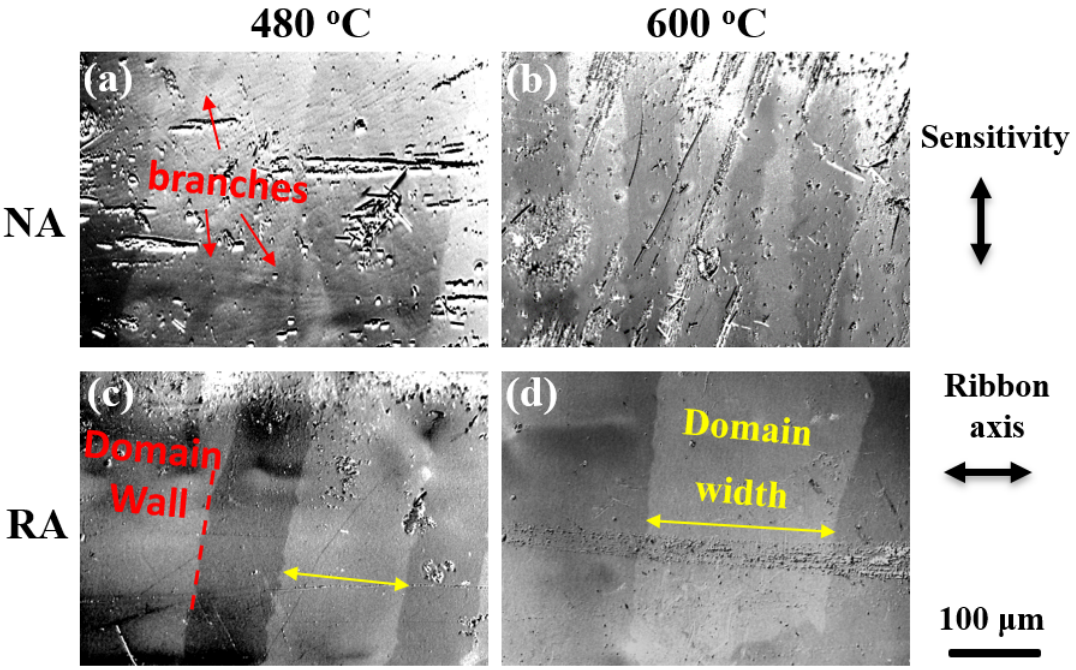

Figure 6. Magnetic domain structure of Mn2 annealed at 480 and 600 °C via (**a**,**b**) NA and (**c**,**d**) RA, respectively.

4. Conclusions

In summary, the effects of the substitution of Mn for Fe as well as rapid annealing on the magnetic softness, thermal stability, microstructure, and magnetic domains of FeSiBNbCu nanocrystalline alloys have been investigated in detail. The addition of 2 at.% Mn and rapid annealing can effectively reduce the H_c and improve the high-frequency μ. The rapid-annealing $Fe_{74}Si_{13}B_8Nb_2Cu_1Mn_2$ alloy exhibits a superb magnetic softness at a large annealing temperature region from 480 to 600 °C, including the relatively high B_s of 1.32 T and low H_c of 1.3~1.4 A/m, together with a large μ at 100 kHz of over 15,000. The improved magnetic softness and thermal stability can be ascribed to the formation of high number density, uniform and fine α-Fe(Si) nano-grains, as well as the regular and wide magnetic domains induced by rapid annealing.

Author Contributions: Conceptualization, A.H.; methodology, B.Z. and A.H.; validation, A.H. and J.L.; formal analysis, B.Z., H.X., and A.H.; investigation, B.Z. and A.H.; resources, Y.D. and F.Y.; data curation, B.Z., H.X., and A.H.; writing—original draft preparation, B.Z.; writing—review and editing, B.Z. and A.H.; visualization, Y.D. and Y.H.; supervision, A.H.; project administration, A.H. and F.Y.; funding acquisition, Y.H. All authors have read and agreed to the published version of the manuscript.

Funding: This work was supported by the China's State Grid Corporation of Science and Technology Projects (5500-201958390A-0-0-00).

Conflicts of Interest: The authors declare no conflict of interest.

References

1. Li, F.C.; Liu, T.; Zhang, J.Y.; Shuang, S.; Wang, Q.; Wang, A.D.; Wang, J.G.; Yang, Y. Amorphous–nanocrystalline alloys: Fabrication, properties, and applications. *Mater. Today Adv.* **2019**, *4*, 100027.
2. Herzer, G. Modern soft magnets: Amorphous and nanocrystalline materials. *Acta Mater*. **2013**, *61*, 718–734.
3. Yoshizawa, Y.; Oguma, S.; Yamauchi, K. New Fe-based soft magnetic alloys composed of ultrafine grain structure. *J. Appl. Phys*. **1988**, *64*, 6044.
4. Suzuki, K.; Makino, A.; Inoue, A.T.; Masumoto, T. High Saturation Magnetization and Soft Magnetic Properties of bcc Fe–Zr–B and Fe–Zr–B–M (M=Transition Metal) Alloys with Nanoscale Grain Size. *Mater. Trans. JIM* **1991**, *32*, 93–102.
5. Lin, X.; Liu, H.; Dou, L.T.; Yang, W.M.; Chang, C.T.; Inoue, A.; Wang, X.M.; Li, R.W.; Shen, B.L. Soft magnetic properties and microstructure of $Fe_{84-x}Nb_2B_{14}Cu_x$ nanocrystalline alloys. *Mater. Des.* **2014**, *56*, 227–231.
6. Liu, L.; Zhou, B.; Zhang, Y.Q.; He, A.N.; Zhang, T.; Li, F.S.; Dong, Y.Q.; Wang, X.M. FeSiBPNbCu Bulk Nanocrystalline Alloys with High GFA and Excellent Soft-Magnetic Properties. *Metals* **2019**, *9*, 219.
7. Willard, M.A.; Laughlin, D.E.; McHenry, M.E.; Thoma, D.; Sickafus, K.; Cross, J.O.; Harris, V.G. Structure and magnetic properties of $(Fe_{0.5}Co_{0.5})_{88}Zr_7B_4Cu_1$ nanocrystalline alloys. *J. Appl. Phys*. **1998**, *84*, 6773–6777.
8. Hasiaka, M.; Fukunaga, H.; Ciurzyn'skab, W.H.; Yamashiro, Y. Effect of Co additon on mircrostructure and magnetic properties of $(Fe_{86-x}Co_x)$-Zr-B alloys. *Scr. Mater.* **2011**, *44*, 1465–1469.
9. Bla´zquez, J.S.; Roth, S.; Mickel, C.; Conde, A. Partial substitution of Co and Ge for Fe and B in Fe–Zr–B–Cu alloys: Microstructure and soft magnetic applicability at high temperature. *Acta Mater.* **2005**, *53*, 1241–1251.
10. Makino, A.; Men, H.; Kubota, T.; Yubuta, K.; Inoue, A. New Fe-metalloids based nanocrystalline alloys with high Bs of 1.9T and excellent magnetic softness. *J. Appl. Phys*. **2009**, *105*, doi:10.1063/1.3058624.
11. Sharma, P.; Zhang, X.; Zhang, Y.; Makino, A. Competition driven nanocrystallization in high Bs and low coreloss Fe–Si–B–P–Cu soft magnetic alloys. *Scr. Mater*. **2015**, *95*, 3–6.
12. Suzuki, K.; Parsons, R.; Zang, B.; Onodera, K.; Kishimoto, H.; Kato, A. Copper-free nanocrystalline soft magnetic materials with high saturation magnetization comparable to that of Si steel. *Appl. Phys. Lett*. **2017**, *110*, doi:10.1063/1.4973772.
13. Wang, J.G.; Zhao, H.; Xie, C.X.; Chang, C.T.; Zhou, S.M.; Feng, J.Q.; Huo, J.T.; Li, W.H. In-situ synthesis of nanocrystalline soft magnetic Fe-Ni-Si-B alloy. *J. Alloys Compd*. **2019**, *790*, 524–528.
14. Parsons, R.; Zang, B.; Onodera, K.; Kishimoto, H.; Shoji, T.; Kato, A.; Suzuki, K. Core loss of ultra-rapidly annealed Fe-rich nanocrystalline soft magnetic alloys. *J. Magn. Magn. Mater*. **2019**, *476*, 142–148.
15. Suzuki, K.; Parsons, R.; Zang, B.; Onodera, K.; Kishimoto, H.; Shoji, T.; Kato, A. Nano-crystallization of amorphous alloys by ultra-rapid annealing: An effective approach to magnetic softening. *J. Alloys Compd*. **2018**, *735*, 613–618.
16. Parsons, R.; Zang, B.; Onodera, K.; Kishimoto, H.; Kato, A.; Suzuki, K. Soft magnetic properties of rapidly-annealed nanocrystalline Fe-Nb-B-(Cu) alloys. *J. Alloys Compd*. **2017**, *723*, 408–417.
17. Ohta, M.; Yoshizawa, Y. Effect of Heating Rate on Soft Magnetic Properties in Nanocrystalline $Fe_{80.5}Cu_{1.5}Si_4B_{14}$ and $Fe_{82}Cu_1Nb_1Si_4B_{12}$ Alloys. *Appl. Phys. Express* **2009**, *2*, 023005.

18. Ohta, M.; Yoshizawa, Y.; Takezawa, M.; Yamasaki, J. Effect of Surface Microstructure on Magnetization Process in $Fe_{80.5}Cu_{1.5}Si_4B_{14}$ Nanocrystalline Alloys. *IEEE Trans. Magn*. **2010**, *46*, 203–206.
19. Jiang, L.X.; Zhang, Y.; Tong, X.; Suzuki, T.; Makino, A. Unique influence of heating rate on the magnetic softness of $Fe_{81.5}Si_{0.5}B_{4.5}P_{11}Cu_{0.5}C_2$ nanocrystalline alloy. *J. Magn. Magn. Mater*. **2019**, *471*, 148–152.
20. Xiao, H.Y.; Wang, A.D.; Zhao, C.L.; He, A.N.; Zhang, G.Y.; Li, H.; Li, R.W.; Liu, X.C. Industrialization of a FeSiBNbCu nanocrystalline alloy with high Bs of 1.39 T and outstanding soft magnetic properties. *J. Mater. Sci. Mater. Electron*. **2018**, *29*, 19517–19523.
21. Wan, F.P.; He, A.N.; Zhang, J.H.; Song, J.C.; Wang, A.D.; Chang, C.T.; Wang, X.M. Development of FeSiBNbCu Nanocrystalline Soft Magnetic Alloys with High B s and Good Manufacturability. *J. Electron. Mater*. **2016**, *45*, 4913–4918.
22. Conde, C.F.; Conde, A.; Svec, P.; Ochin, P. Influence of the addition of Mn and Cu on the nanocrystallization process of HITPERM Fe–Co–Nb–B alloys. *Mater. Sci. Eng. A* **2004**, *375–377*, 718–721.
23. Conde, C.F.; Franco, V.; Conde, A.; Kiss, L.F. Microstructure and magnetic permeability of Hitperm (FeMn)CoNbB(Cu) alloys. *J. Magn. Magn. Mater*. **2004**, *272–276*, 1430–1432.
24. Millán, M.; Blázquez, J.S.; Conde, C.F.; Conde, A.; Lozano-Pérez, S.; Ochin, P. Preferential Co partitioning to α-Fe in nanocrystalline CoFeNbB alloys by Mn addition. *J. Non-Cryst. Solids*. **2009**, *355*, 109–113.
25. Chen, Y.M.; Ohkubo, T.; Ohta, M.; Yoshizawa, Y.; Hono, K. Three-dimensional atom probe study of Fe–B-based nanocrystalline soft magnetic materials. *Acta Mater*. **2009**, *57*, 4463–4472.
26. Akira, T.; Inoue, A. Classification of Bulk Metallic Glasses by Atomic Size Difference, Heat of Mixing and Period of Constituent Elements and Its Application to Characterization of the Main Alloying Element. *J. Appl. Phys*. **2005**, *46*, 2817–2829.
27. McHenry, M.E.; Willard, M.A.; Laughlin, D.E. Amorphous and nanocrystalline materials for applications as soft magnets. *Prog. Mater Sci*. **1999**, *44*, 291–433.
28. Dobák, S.; Füzer, J.; Kollár, P.; Strečková, M.; Bureš, R.; Fáberová, M. A comprehensive complex permeability approach to soft magnetic bulk cores from pure or resin coated Fe and pulverized alloys at elevated temperatures. *J. Alloys Compd*. **2017**, *695*, 1998–2007.
29. Edwards, A.J.; Klug, H.P.; Alexander, L.E. *X-ray Diffraction Procedures for Polycrystalline and Amorphous Materials*, 2nd ed.; Wiley-Interscience: New York, NY, USA, 1974; p. 992, ISBN 0-471-49369-4.
30. Flohrer, S.; Herzer, G. Random and uniform anisotropy in soft magnetic nanocrystalline alloys (invited). *J. Magn. Magn. Mater*. **2010**, *322*, 1511–1514.